SYSTEMATIC AND RANDOM ERRORS FOR MAIN INJECTOR TRACKING

Fady A. Harfoush
Shekhar Mishra

October 31, 1991

1 Introduction

The calculation of magnetic field errors, both systematic and random, closed orbit errors, and other parameters needed to track the Main Injector lattice MI17 are described in this paper. Tracking will be performed at injection (8.9 GeV/c), transition (21.5 GeV/c), slow extraction (120 GeV/c), and coalescing (150 GeV/c) using the code TPOT. Results will be the subject of another MI note. Whenever possible, measured field multipoles [1] are compared to the PE2D calculations [2]. Eddy current measurements have not yet been performed. This question will be addressed in a future MI note.

At the Fermilab Magnet Test Facility measurements of the magnet field shape and field quality have been performed. The tracking of the Main Injector (MI) lattice requires a detailed knowledge of the magnetic field quality and its variation from magnet to magnet. As of the date of this report only two MI dipoles have been built IDM001 and IDM002. Since field measurements of only two magnets are not enough for statistical analysis, we have used the data from the Main Ring B2 dipoles. The data were obtained with a rotating coil and measured at 97 A, 210 A, and 1700 A. The rotating coil was placed at the center of the magnet ($x = y = 0$) to measure the body field multipoles. The B2 dipole strength is obtained from a flat coil measurement 1″ wide. The new MI dipoles have been measured by a Hall probe, NMR probe, Rotating coil, and Flat coil probe. The Hall and NMR probe measures field at any (x, y, z) location in the magnet. The rotating coil is a cylindrical probe of radius 0.86" with wire windings on the surface and measures the integrated (over the length of the probe) multipoles of the magnet. These measurements are later scaled to 1" radius. The flat coil is a probe with several coil wound around a rectangular frame. The probe measures the integrated relative flux as a function of position by translation of the probe. It can also measure the integrated relative flux as a function of magnet current.

2 Systematic Errors in Dipoles End and Body Multipoles

2.1 Integrated End Field Using Flat Coils

Three different methods for measuring the integrated end field using flat coils are presented. The first method is a direct measurement where one end of the flat coil is exactly at one end of the magnet as shown in Fig. 1a. The rest of the flat coil is completely outside the magnet. The second method, shown in Fig. 1b, takes a series of measurements where one end of the flat coil is gradually pushed inside the magnet. A plot of the integrated end field versus the length of the flat coil inside the magnet is thus obtained. By extrapolating to zero length the end effect is calculated. The third method, described below, considers a combined flat coil measurement of the end and body fields

and a flat coil measurement of the body field. Referring to Fig. 1c the sum of the integrated field of both ends is:

$$\int_{-z}^{0} Bdl + \int_{L}^{L+z} Bdl = \int_{-z}^{L+z} Bdl - \int_{0}^{L} Bdl \quad (1)$$

Here $L = 20'$, the physical length of the magnet. The first right hand term of the equal sign is the flux measured using a $24'$ long flat coil. The second term, to a good approximation, is equal to the measurement obtained using a $16'4''$ long flat coil and scaled by the factor $\frac{L_{20'}}{L_{16'4''}}$. Following a notation more descriptive of the available measurements the above equation is rewritten as:

$$\int_{ends} Bdl \sim \int_{L_{24'}} Bdl - (\int_{L_{16'4''}} Bdl) \times \frac{L_{20'}}{L_{16'4''}} \quad (2)$$

On the other hand,

$$\int_{24'} Bdl = B_o L_{eff} \quad (3)$$

$$\int_{L_{20'}} Bdl \sim B_o L_{20'} \quad (4)$$

and so

$$\int_{ends} Bdl \sim B_o(L_{eff} - L_{20'}) \quad (5)$$

where L_{eff} is defined as:

$$L_{eff} = \frac{\int_{L_{24'}} Bdl \times L_{16'4''}}{\int_{L_{16'4''}} Bdl} \quad (6)$$

With the existing end shape of the new MI dipoles L_{eff} is always smaller than $L_{20'}$ and so the quantity in eq. 5 is always negative. Equation 6 is used to calculate the effective length of the two prototype magnets at different currents as shown in Fig. 6.

Comparative results are shown in Table 2. The error in the field[1] measured using flat coils is of the order of $\sim 1\%$ of the field value. This number is roughly equal to the ratio of one coil thickness to the total thickness of the coils. With this in mind, the agreement between the first two methods is good. The results of the third method, referred to as indirect, should be treated differently from the first two. This is the end effect for a field assumed uniform along the physical length of the dipole magnet. It is an end correction for a perfect dipole magnet. This method is more suitable for tracking because it preserves the physical length of the magnet as defined in the MI17 lattice. Any other method would require defining a new physical length to be associated with the uniform field region and this can lead to some confusion. For tracking purposes we will select the multipoles of the integrated end field as calculated from the indirect method. This is described in the next section.

2.2 Integrated End Multipoles Using Rotating Coils

For the calculation of the integrated end multipoles we refer to Fig 1d where $L_e = L_b = 80''$ ($30''$ inside the magnet and $50''$ outside), $L = 240''$, and $L_o = 180''$. Measurements of the end and body fields are made separately. The integrated end multipoles are calculated from the measured

[1] H.Glass

quantities $\int_{L_e} B_o dl$, $\int_{L_b} B_o dl$, $\int_{L_e} B_n dl$, and $\int_{L_b} B_n dl$. Let us define:

$$p_n \text{ or } q_n = \frac{\int_{L_e} B_n dl}{\int_{L_e} B_o dl} \tag{7}$$

$$v_n = \frac{\int_{L_b} B_n dl}{\int_{L_b} B_o dl} \tag{8}$$

The variables p_n and q_n refer respectively to the lead end and other end measurements, and v_n to the body measurements. Similar to Eq. 1 the integrated end multipole for either end is:

$$\int_{Lend} B_n dl = (p_n, q_n) \int_{L_e} B_o dl + v_n \int_{L_b} B_o dl (\frac{L_o - L}{2L_b}) \tag{9}$$

In terms of relative units ($\times 10^4$u. at 1") similar to the body field multipoles, we have:

$$B_n = \frac{\int_{Lend} B_n dl}{B_o Lend} \tag{10}$$

where $Lend = 50''$.

The MI17 lattice will be modified to include separate integrated multipole elements at each end of a dipole. The ends will have only systematic errors due to the iron saturation and its shape. Random errors will be added to the body fields measurements.

2.3 Body Field Profile Using Flat Coils and Rotating Coils

Multipoles of a rotating coil measurement are used to reconstruct the field in a circular region centered with the rotating coil and with a radius equal to the radius of convergence of the corresponding Taylor series. For a rotating coil centered in the gap of the dipole magnet this radius is equal to 1", the distance from the center to the closest pole face. Beyond the radius of convergence the multipoles are derived from a least square polynomial fit to the field profile. This latter is obtained either from overlapping rotating coil or flat coil measurements. In [3] a polynomial fit in 1-D (x as the horizontal variable) was used when it was found that the tracking results were in disagreement with what has been observed in the Main Ring. The level of disagreement was significantly reduced when the coefficients obtained from a 1-D polynomial fit were used instead of the measured multipoles. A least square fit to the field in a 2-D region is also possible. Results[2] have shown, as one might expect, that the number of coefficients needed to best describe the field in a 2-D region grows very rapidly as one approaches the edges of the region under consideration.

Body field profiles of the new prototype dipoles are reconstructed for x varying between $[-1'', 1'']$ and $[-2'', 2'']$ using three overlapping rotating coil and flat coil measurements. The coefficients of a 7th order polynomial fit to the flat coil measurements at 9500 A and 7000 A are given in Table 3. At low currents, 1500 A and 498 A, the field profiles obtained from the flat coil measurements are not suitable for fitting. Instead we used overlapping coil measurements to reconstruct the field profile and a 10th order polynomial fit to obtain the coefficients.

2.4 Dipole Error due to Variations in Effective Length

Fig. 6 is a plot of the effective length versus current excitation for IDM001, and IDM002 dipoles without the remanent field correction. The remanent field correction is expected to bring the

[2] M. Foley,F. Harfoush, and J.F.Ostiguy

diverging curve at low currents closer to the straight lines. In going from low energies to high energies the maximum change in effective length is about 8 mm. This should be compared to preliminary calculations[3] which give around 6.5 mm. Let θ_o, expected to be equal to $\frac{2\pi}{904/3}$, be the nominal bending angle at 120 GeV for which $L_{eff} = L_{ref}$. At energies other than 120 GeV the dipole bending angle will vary due to a change in the effective length. To correct for this change a factor ϵ is added where now:

$$\theta_l = (1+\epsilon)(1+\frac{\triangle L}{L_{ref}})\theta_o \quad \text{for long dipole} \tag{11}$$

$$\theta_s = \frac{2}{3}(1+\epsilon)(1+\frac{3}{2}\frac{\triangle L}{L_{ref}})\theta_o \quad \text{for short dipole} \tag{12}$$

The correction factor ϵ is defined such that the closed orbit relation:

$$2\pi = N_l\theta_l + N_s\theta_s \tag{13}$$

is satisfied. N_l and N_s are respectively the numbers of long and short dipoles. For $\epsilon \ll 1$ one can neglect the cross terms in ϵ and $\frac{\triangle L}{L_{ref}}$. After substitution ϵ becomes equal to:

$$\epsilon = \frac{(N_l+N_s)f}{(N_l+N_s)f + (N_l+\frac{2}{3}N_s)} \tag{14}$$

where $f = \frac{\triangle L}{L_{ref}}$ is the relative change in the effective length for the long dipole. It is assumed that the absolute change in effective length is the same for both long and short dipoles. Given the above relations one can calculate to a first order approximation the corresponding change in dipole field as:

$$\frac{\triangle B}{B_o} \simeq \epsilon + f \quad \text{for long dipole}$$

$$\frac{\triangle B}{B_o} \simeq \frac{2}{3}\epsilon + f \quad \text{for short dipole}$$

L_{ref} is obtained from the solid line in Fig. 6 and is equal to $6.0462m$. At injection this value becomes $6.0492m$. This gives an $\epsilon = 5.6 \times 10^{-4}$. The field change due to ϵ is a systematic body error while the field change due to f is a systematic end error. This latter has already been included in the calculations of the integrated end field described in sections 2.1 and 2.3.

3 Random Errors in Body Multipoles

Up to now we have only considered systematic errors in the end and body fields of the dipole magnets. For the random multipole errors we will use the measurements of the Main Ring B2 dipoles. However it was brought to our attention[4] that a fraction of the random error is caused by the measurement technique, which has improved over the past few years. Therefore the random errors derived from the B2 measurements are expected to be a worst case scenario for the new dipoles. The random errors in the dipole field, as mentionned in the introduction, are calculated from flat coil measurements. We will use the random errors of the B2 dipoles at 210 A to track the MI at injection and transition. The random errors at 1700 A will be used to track the MI at

[3] J.F.Ostiguy

[4] Bruce Brown

slow extraction and coalescing even though the magnet begins to saturate. Another issue brought to our attention[5] is the fact that half of the B2 dipoles have coil end in a plane opposite to the other half. The result is a skew quadrupole positive for half the dipoles and negative for the rest. This is not the case with the new dipoles and so the random error in the skew quadrupole should be calculated using half of the B2 dipoles for which the coil end is in the same plane as the new dipoles.

The random errors for the "New Style" MR quads are calculated using existing measurements. It is noted the variations with current of the octopole systematic and random errors are small.

4 Closed Orbit Random Errors

The closed orbit errors caused by random misalignments and field errors are given in Table 1. In generating Table 1 the following numbers have been assumed:

- Dipole strength error $\frac{\triangle B}{B_0} \mid_{rms} = 7 \times 10^{-4}$ at all energies
- RMS roll angle = 0.50 mrad $(\frac{25\mu m}{5cm})$
- Bending angle per dipole = $\frac{2\pi}{904/3} = \sim 20.85 mrad$
- Four dipoles per cell

The tracking code TPOT allows for random displacement errors and angular rotation errors. One should note that the random error calculated from the B2 dipole measurements is different from the above suggested value of 7×10^{-4} . At 150, 120 GeV/c the value is 2.5×10^{-3}, and at 21.5, 8.9 GeV/c the value is 2.3×10^{-3}.

Quadrupole & BPM Displacement Errors	Dipole Errors	
	Strength (H-plane)	Rotation (V-plane)
$(\triangle x)_{rms} = (\triangle y)_{rms} = 0.25mm$	$(\triangle\theta)_{rms} = 0.0206mrad$ at all energies	$(\triangle\theta)_{rms} = 0.0147mrad$

Table 1: Orbit errors

5 Brief Summary and Results

To summarize the dipole field including systematic and random errors is represented as:

$$B_y(x, y = 0) = B_o(b_o \mid_\epsilon + \sum_0^\infty (B_n + \sigma_n) \mid_{body} + B_n \mid_{end1} + B_n \mid_{end2}) x^n \qquad (15)$$

where $b_o \mid_\epsilon$ is the relative systematic dipole due to a change in the strength of the bending angle,B_n is the systematic body field multipole, σ_n is the rms random error associated with the body field, and $B_n \mid_{end1,2}$ are the systematic multipoles at each end of the magnet.

The measured field multipoles, both normal and skew, for a long MI dipole and a "New Style" MR quadrupole are plotted in Figures 2-5. Listed in Tables 4-11 are the allowed multipole errors at the four desired energies, including the skew multipoles. The non allowed multipoles, as seen from Figures 2-5, are of the order of 10^{-5} in relative magnitude. This is almost at the noise level

[5]Stan Pruss

of the measurements and therefore are not included. The only non allowed multipole to watch for is the quadrupole component in the dipole magnets due to the backleg gap. This problem has been studied in [2]. In each table the dipole field is expressed in Tesla (T), the quadrupole in Tesla per inch (T/in), and the higher order multipoles in relative units $\times 10^4$ (u). The reference radius is $r = 1$ in. The multipoles are numbered such that b_0 corresponds to the dipole, b_1 to the quadrupole, b_2 to sextupole, b_3 to octopole, b_4 to decapole, etc..... Here b_n refers to a normal multipole and a_n to a skew multipole. Skew multipoles in quadrupoles are not listed because they can be easily corrected for.

6 Other Tracking Parameters

Tracking will be performed at only injection, transition, and coalescing as mentionned in the memo by Holmes, and Peggs [5]. The following momentum offsets, obtained from [6], RF voltages obtained from [7], and corrected chromaticity will be used.

- At injection (E=8.9 GeV) $\frac{\partial p}{p} = 2 \times 10^{-3}$ for 35,000 turns, with $V_{rf} = 0.393$ MV. Vertical and horizontal chromaticities ζ_v, ζ_H corrected to -5, -5.
- At transition ($\gamma_t = 21.59$, E=21.5 GeV) $\frac{\partial p}{p} = 10 \times 10^{-3}$ for 1000 turns. Vertical and horizontal chromaticities ζ_v, ζ_H corrected to -20,-20 and +20,+20.
- At coalescing (E=150 GeV) $\frac{\partial p}{p} = 10^{-3}$ for 50,000 turns, and $\frac{\partial p}{p} = \frac{1}{3} \times 10^{-3}$ for 100,000 turns with $V_{rf} = 0.534$ MV. Vertical and horizontal chromaticities ζ_v, ζ_H corrected to +5,+5.

For each case the RF frequency is set to 54 MHz corresponding to a harmonic number of 588. Similar to MI16, the machine fractional tune is set to 0.407 in the horizontal plane and 0.409 in the vertical plane.

References

[1] Henry Glass, *Private Communication.*

[2] Jean-François Ostiguy, *MI-0036, MI-0041*, October 1990.

[3] R. Gerig, *Fermilab Upgrade Phase II: The Main Injector*, January 1990.

[4] S. M. Pruss, et al, *Harmonic Analysis of Fermilab Main Ring Quadrupoles*, Proceedings of the IEEE 1991 Particle Accelerator Conference.

[5] Steve Holmes, Steve Peggs, *Internal Memo*, September 1991.

[6] Conceptual Design Report, *Revision 2.3, Addendum*, p. 16, March 1991.

[7] Philip S. Martin, *MI-0027A*, December 1990.

Current (A)	Integrated End Field (T-m)			
	Direct Meas. of Other End	Extrapolation		Indirect Meas. of Both Ends
		Lead End	Other End	
500	0.00207	0.0004	0.00128	-0.002
1500	0.00628	0.0013	0.00381	-0.0077
7000	0.0291	0.0130	0.01906	-0.0394
9500	0.0376	0.0034	0.02276	-0.0518

Table 2: Integrated end field using three methods of calculations

Current (A)	Fit for 1" (in u.)	Fit for 2"(in u.)
	b_o = 0.0095	-0.287
	b_1 = -0.1230	-0.185
	b_2 = -9.184	-8.039
9500	b_3 = 0.168	-0.0936
	b_4 = -1.402	-2.509
	b_5 = -0.258	-0.0562
	b_6 = -0.106	-0.183
	0.0092	-0.0779
	0.138	0.0514
	-1.15	-1.921
	-0.0832	0.107
7000	-0.151	0.979
	0.0449	-0.0421
	-0.0665	-0.461
	0.000346	-0.002657
	-0.00977	-0.07620
	0.61952	0.6945
1500	-0.2541	-0.0591
	0.2262	0.0369
	0.1469	0.2031
	-0.1339	-0.1486
	0.000786	-0.00591
	-0.00418	-0.0480
	0.5593	0.695
500	-0.1779	-0.1277
	0.2235	-0.0386
	0.00499	0.237
	-0.0226	-0.10311

Table 3: Coefficients of a polynomial fit to a body field profile at different currrents

	Dipole Systematic and Random Multipole Errors		
	Body (Calc.) Measured at 9.5 kA	Lead End	Other End
Long MI Dipoles N = 216 L = 6.096 m (2 Prototypes)	$b_0 = (1.742)\ 1.761 \pm 0.00442T$ $b_2 = (-9.495) - 11.392 \pm 0.4187u.$ $a_2 = -0.0812 \pm 0.1767u.$ $b_4 = (-1.323) - 1.311 \pm 0.2913u.$ $a_4 = -0.0385 \pm 0.0675u.$ $b_6 = (-0.0618) - 0.313 \pm 0.2111u.$ $a_6 = -0.0812 \pm 0.0769u.$ $b_8 = -0.0594 \pm 0.1870u.$ $a_8 = 0.129 \pm 0.0730u.$ $b_{10} = -0.0186 \pm 0.1760u.$ $a_{10} = -0.0882 \pm 0.0766u.$	$0.0151 \pm 0T$ $5.599 \pm 0u.$ $-0.171 \pm 0u.$ $-0.578 \pm 0u.$ $-0.0572 \pm 0u.$ $-0.391 \pm 0u.$ $-0.0483 \pm 0u.$ $-1.00493 \pm 0u.$ $-0.0748 \pm 0u.$ $0.117 \pm 0u.$ $0.0821 \pm 0u.$	$-0.0155 \pm 0T$ $6.258 \pm 0u.$ $-0.180 \pm 0u.$ $-0.538 \pm 0u.$ $-0.161 \pm 0u.$ $-0.411 \pm 0u.$ $-0.133 \pm 0u.$ $-0.00751 \pm 0u.$ $-0.118 \pm 0u.$ $0.0691 \pm 0u.$ $0.0257 \pm 0u.$
Short MI Dipoles N = 128 L = 4.064 m (Not built yet)	Use above	Use above	Use above

Table 4: Dipole at Coalescing

	Quadrupole Systematic and Random Multipole Errors
	Body (Calc. at 3.630 kA)+End Measured at 3.5 kA
"New Style" MR Quads L = 2.1336 m N = 128	$b_1 = (0.532)0.5062 \pm 0.00136T/in$ $b_3 = (8.847)5.405 \pm 1.804u.$ $b_5 = (-1.345) - 1.706 \pm 0.256u.$ $b_7 = (1.421)u.$ $b_9 = (-0.783) - 0.899 \pm 0.0523u.$
New MI Quads N=32 L=2.5 m N=48 L=2.953 m (Not built yet)	$b_1 = (0.531)T/in$ $b_3 = (-0.119)u.$ $b_5 = (-1.443)u.$ $b_7 = (1.304)u.$ $b_9 = (-0.772)u.$

Table 5: Quadrupole at Coalescing.

	Dipole Systematic and Random Multipole Errors		
	Body (Calc.) Meas. at 7.00 KA	Lead End Meas.	Other End Meas.
Long MI Dipoles N = 216 L = 6.096 m (2 Prototypes)	$b_0 = (1.382)1.366 \pm 0.00343T$ $b_2 = (-0.975) - 1.336 \pm 0.4187u.$ $a_2 = -0.0354 \pm 0.1767u.$ $b_4 = (-0.048) - 0.112 \pm 0.2913u.$ $a_4 = -0.0496 \pm 0.0675u.$ $b_6 = (-0.018) - 0.0983 \pm 0.2111u.$ $a_6 = -0.0631 \pm 0.0769u.$ $b_8 = -0.0455 \pm 0.1870u.$ $a_8 = 0.0998 \pm 0.0730u.$ $b_{10} = 0.0024 \pm 0.1760u.$ $a_{10} = -0.0536 \pm 0.0766u.$	$0.0203 \pm 0T$ $5.653 \pm 0u.$ $-0.0777 \pm 0u.$ $-0.477 \pm 0u.$ $-0.0181 \pm 0u.$ $-0.469 \pm 0u.$ $-0.132 \pm 0u.$ $-0.164 \pm 0u.$ $-0.155 \pm 0u.$ $-0.0831 \pm 0u.$ $0.161 \pm 0u.$	$-0.00826 \pm 0T$ $5.909 \pm 0u.$ $-0.131 \pm 0u.$ $-0.494 \pm 0u.$ $-0.142 \pm 0u.$ $-0.440 \pm 0u.$ $-0.112 \pm 0u.$ $-0.00173 \pm 0u.$ $0.0245 \pm 0u.$ $-0.0538 \pm 0u.$ $0.0210 \pm 0u.$
Short MI Dipoles N = 128 L = 4.064 m (Not buit yet)	Use above	Use above	Use above

Table 6: Dipole at Slow Extraction

	Quadrupole Systematic and Random Multipole Errors
	Body(Calc. at 2.904 kA)+End Measured at 3.0 kA
"New Style" MR Quads L = 2.1336 m N = 128	$b_1 = (0.428)0.4355 \pm 0.00103T/in$ $b_3 = (9.109)5.291 \pm 1.289u.$ $b_5 = (-1.342) - 1.6322 \pm 0.2146u.$ $b_7 = (1.377)u.$ $b_9 = (-0.802) - 0.8532 \pm 0.0989u.$
New MI Quads N=32 L=2.5 m N=48 L=2.953 m (Not built yet)	$b_1 = (0.427)T/in$ $b_3 = (-0.0964)u.$ $b_5 = (-1.407)u.$ $b_7 = (1.316)u.$ $b_9 = (-0.738)u.$

Table 7: Quadrupole at Slow Extraction.

	Dipole Systematic and Random Multipole Errors		
	Body Meas. at 1.51 kA	Lead End Meas.	Other End Meas.
Long MI Dipoles N = 216 L = 6.096 m (2 Prototypes)	$b_0 = 0.2959 \pm 0.000536T$ $b_2 = 0.5559 \pm 0.6123u.$ $a_2 = -0.04301 \pm 0.2206u.$ $b_4 = 0.02248 \pm 0.3148u.$ $a_4 = -0.01237 \pm 0.1464u.$ $b_6 = -0.03076 \pm 0.2287u.$ $a_6 = -0.06130 \pm 0.0826u.$ $b_8 = -0.04614 \pm 0.2521u.$ $a_8 = 0.07242 \pm 0.1534u.$ $b_{10} = -0.0045 \pm 0.2151u.$ $a_{10} = -0.058 \pm 0.0875u.$	$-0.0051 \pm 0T$ $4.924 \pm 0u.$ $1.1051 \pm 0u.$ $0.05055 \pm 0u.$ $-0.366 \pm 0u.$ $-0.763 \pm 0u.$ $-0.01703 \pm 0u.$ $1.0374 \pm 0u.$ $0.6000 \pm 0u.$ $-0.221 \pm 0u.$ $-1.114 \pm 0u.$	$-0.019 \pm 0T$ $5.584 \pm 0u.$ $-0.0814 \pm 0u.$ $-0.459 \pm 0u.$ $-0.178 \pm 0u.$ $-0.4036 \pm 0u.$ $0.0965 \pm 0u.$ $0.00824 \pm 0u.$ $-0.0494 \pm 0u.$ $0.0239 \pm 0u.$ $0.0119 \pm 0u.$
Short MI Dipoles N = 128 L = 4.064 m (Not built yet)	Use above	Use above	Use above

Table 8: Dipole at Transition

	Quadraple Systematic and Random Multipole Errors
	Av. Body+End Measured at 0.5 kA
"New Style" MR Quads L = 2.1336 m N = 128	$b_1 = 0.07259 \pm 0.000327T/in$ $b_3 = 4.899 \pm 1.456u.$ $b_5 = -1.5707 \pm 0.36u.$ $b_7 =$ $b_9 = -0.8644 \pm 0.1007u.$
New MI Quads N=32 L=2.5 m N=48 L=2.953 m (Not built yet)	Not Available

Table 9: Quadrupole at Transition

	Dipole Systematic and Random Multipole Errors		
	Body(Calc.)Meas. at 0.498 kA	Lead End Meas.	Other End Meas.
Long MI Dipoles N = 216 L = 6.096 m (2 Prototypes)	$b_0 = (0.0992)0.0979 \pm 0.000177T$ $b_2 = (0.2200)0.5118 \pm 0.6123u.$ $a_2 = -0.04677 \pm 0.2206u.$ $b_4 = (0.1839)0.2199 \pm 0.3148u.$ $a_4 = 0.0302 \pm 0.1464u.$ $b_6 = (-0.0403) - 0.0131 \pm 0.2287u.$ $a_6 = -0.0575 \pm 0.0826u.$ $b_8 = -0.0367 \pm 0.2521u.$ $a_8 = 0.1232 \pm 0.1534u.$ $b_{10} = 0.0309 \pm 0.2151u.$ $a_{10} = -0.0396 \pm 0.0875u.$	$-0.0529 \pm 0T$ $0.229 \pm 0u.$ $0.123 \pm 0u.$ $0.146 \pm 0u.$ $-0.0699 \pm 0u.$ $-0.0699 \pm 0u.$ $0.0418 \pm 0u.$ $0.124 \pm 0u.$ $-0.0482 \pm 0u.$ $-0.0450 \pm 0u.$ $-0.0804 \pm 0u.$	$-0.0529 \pm 0T$ $0.286 \pm 0u.$ $0.0152 \pm 0u.$ $0.0972 \pm 0u.$ $-0.0377 \pm 0u.$ $-0.0418 \pm 0u.$ $0.0418 \pm 0u.$ $0.0192 \pm 0u.$ $-0.0812 \pm 0u.$ $-0.0185 \pm 0u.$ $0.0128 \pm 0u.$
Short MI Dipoles N = 128 L = 4.064 m (Not built yet)	Use above	Use above	Use above

Table 10: Dipole at Injection

	Quadrupole Systematic and Random Multipole Errors
	Av. Body (Calc. at 0.215 kA)+End Meas. at 195 kA)
"New Style" MR Quads L = 2.1336 m N = 128	$b_1 = (0.0319)T/in$ $b_3 = (9.390)5.854 \pm 1.0203u.$ $b_5 = (-1.276) - 1.8218 \pm 0.6312u.$ $b_7 = (1.410)u.$ $b_9 = (-0.752) - 0.8023 \pm 0.0642u.$
New MI Quads N=32 L=2.5 m N=48 L=2.953 m (Not built yet)	$b_1 = (0.0317)T/in$ $b_3 = (-0.394)u.$ $b_5 = (-1.397)u.$ $b_7 = (1.295)u.$ $b_9 = (-0.727)u.$

Table 11: Quadrupole at Injection.

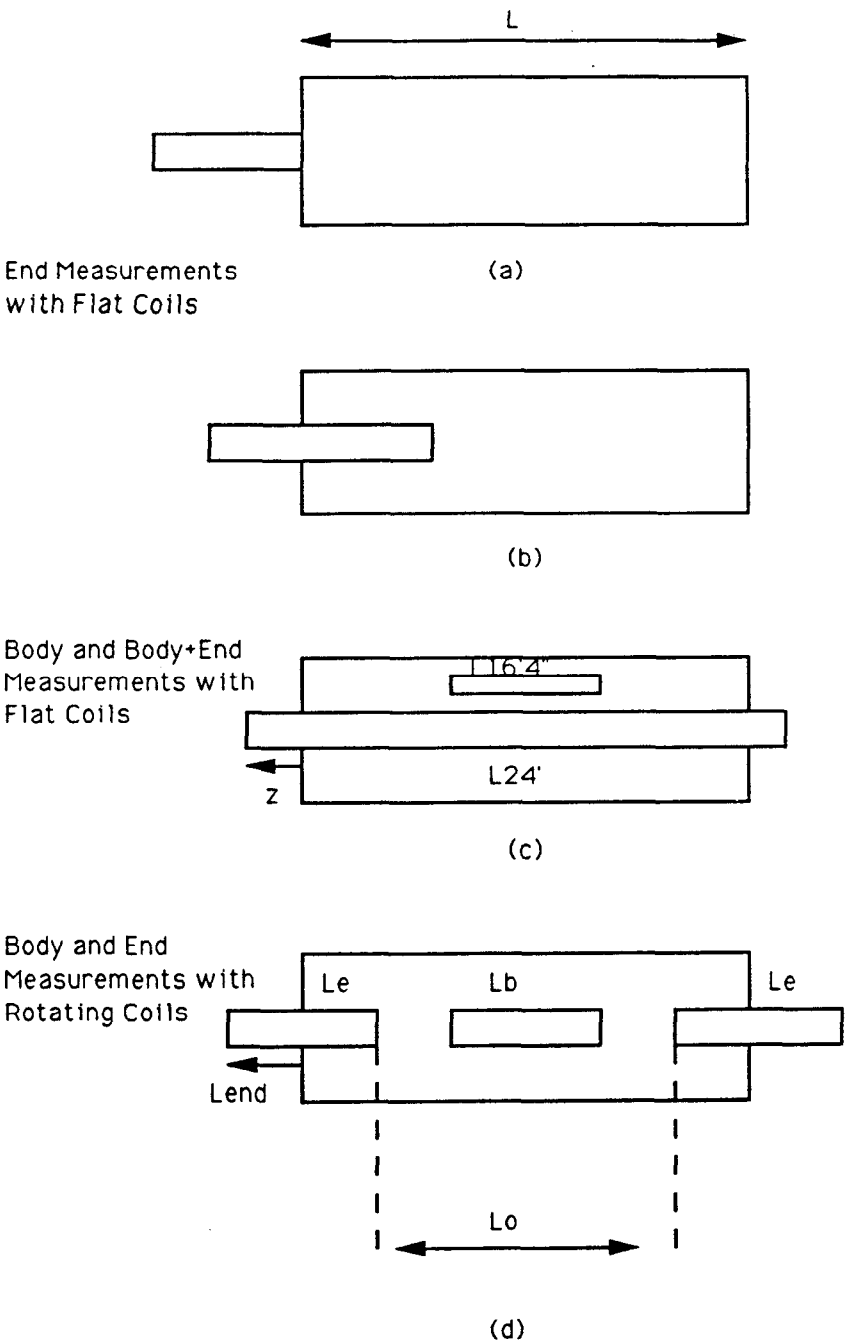

Figure 1: End and body field measurements setup

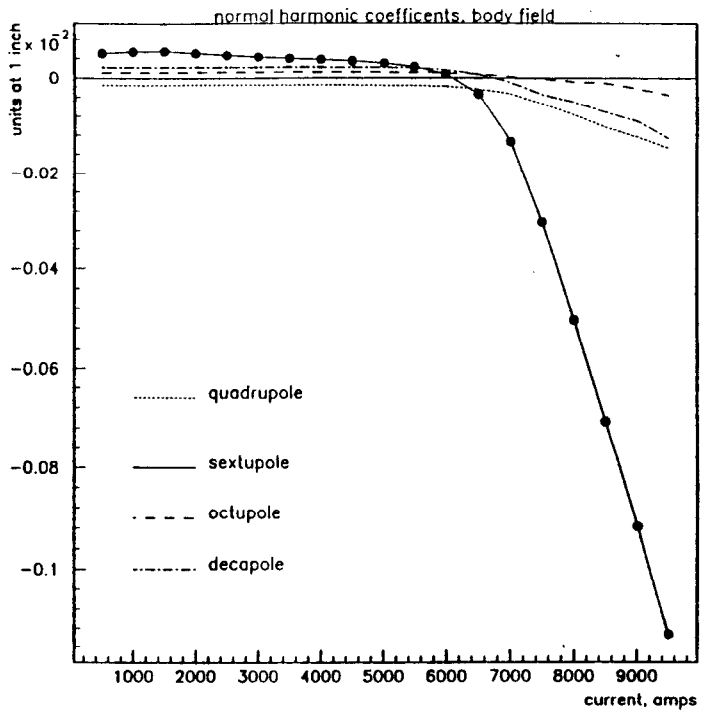

Figure 2: Normal harmonic coefficients vs current for long dipole

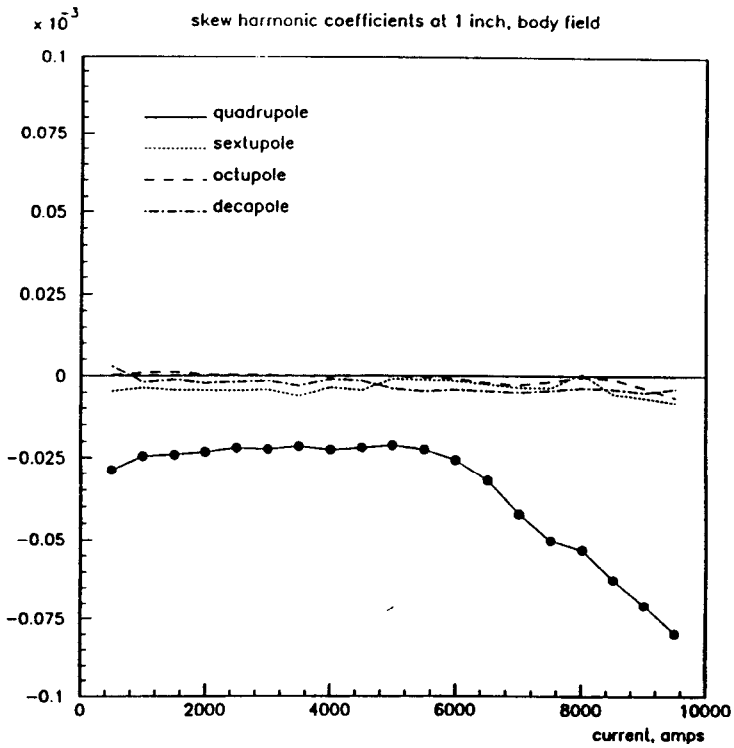

Figure 3: Skew harmonic coefficients vs current for long dipole

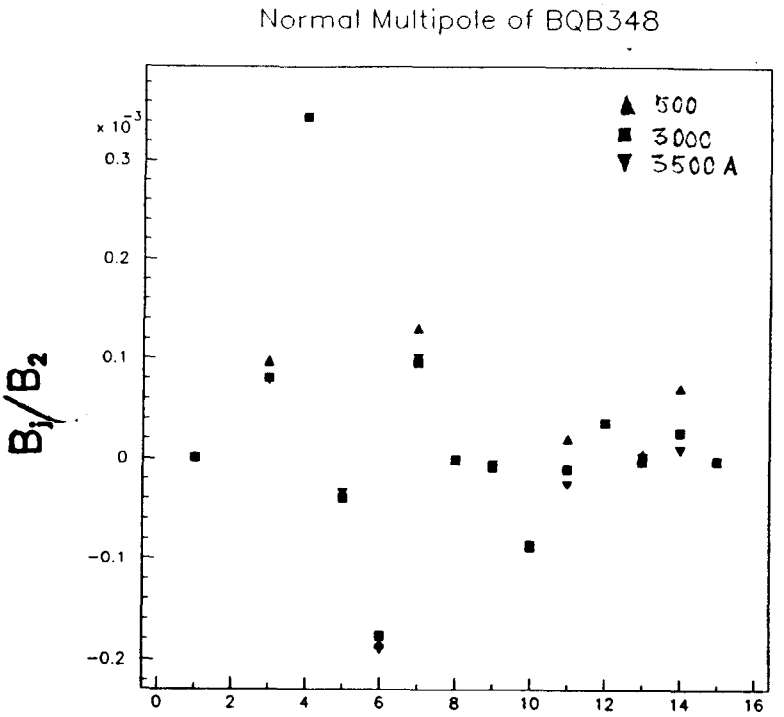

Figure 4: Normal harmonic coefficients for different multipoles (Here n=2 is quadrupole)

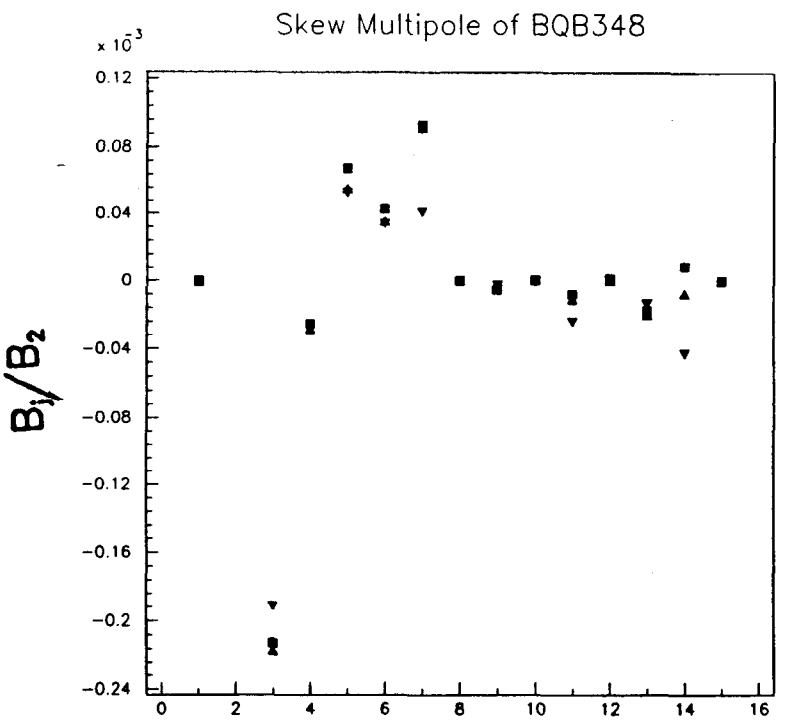

Figure 5: Skew harmonic coefficients for different multipoles (Here n=2 is quadrupole)

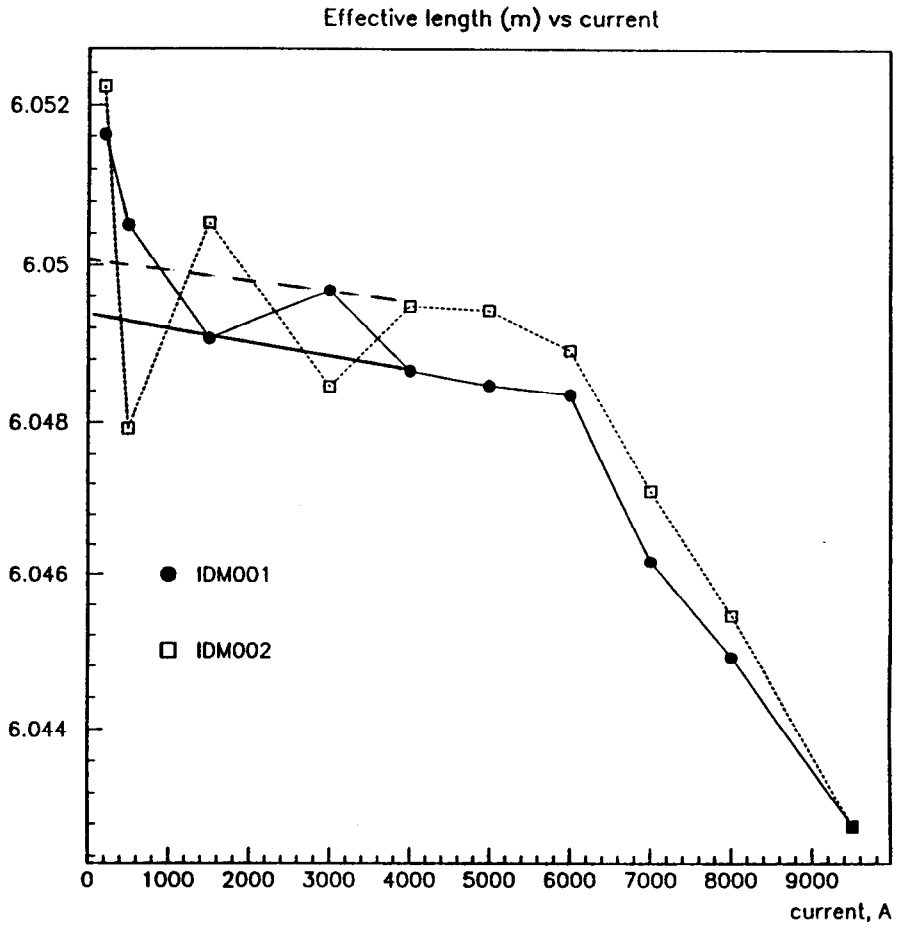

Figure 6: Effective length (m) vs current